iJRASET
International Journal For Research in Applied Science and Engineering Technology

INTERNATIONAL JOURNAL FOR RESEARCH

IN APPLIED SCIENCE & ENGINEERING TECHNOLOGY

Volume: 12 **Issue:** VI **Month of publication:** June 2024

DOI: https://doi.org/10.22214/ijraset.2024.63195

www.ijraset.com

Call: 08813907089 | E-mail ID: ijraset@gmail.com

International Journal for Research in Applied Science & Engineering Technology (IJRASET)
ISSN: 2321-9653; IC Value: 45.98; SJ Impact Factor: 7.538
Volume 12 Issue VI June 2024- Available at www.ijraset.com

Investigation of the Structural, Electrical, and Optical Properties of Co-Precipitation-Synthesized Aluminum-Doped ZnO Nanostructures

Sowmya Kanakamedala[1], Aparna Yarramareddy[2]
[1]*Department of Physics, BVRIT HYDERABAD College of Engineering for Women, Telangana, Hyderabad, India*
[1, 2]*Department of Physics, Jawaharlal Nehru Technological University, Hyderabad, Telangana, India*

Abstract: ***This study examines the Structural, Electrical, and Optical characteristics of Zinc Oxide substituted with aluminum ($Al_xZn_{1-x}O$; x = 0, 0.02, 0.04, 0.06, 0.08). The coprecipitation technique is used to synthesize the powders, and X-ray diffraction (XRD) is used to analyze the powders' structural properties. Field Emission Scanning Electron Microscopy (FESEM) is used to study the morphological characteristics of the produced powders. The UV-visible absorbance spectrum (UV-Vis.) was used to assess the particles' optical characteristics. Using photoluminescence (PL) spectra, the effects of morphology on the optical and electrical characteristics of produced powders were examined. The XRD patterns verified that a single-phase hexagonal wurtzite structure formed for each sample. The powders' FESEM pictures reveal how, as the Al concentration increases, the particles' morphology alters from hexagonal to spherical. The synthesized samples have crystallite sizes between 19 and 26 nm. The predictable variations noticed with Al^{3+} concentration are consistent with Al^{3+} incorporation into the ZnO lattice, as confirmed by the UV-Vis spectroscopy measurements.***

Keywords: Aluminum-substituted zinc oxide, Structural properties, Coprecipitation technique, Photoluminescence (PL) spectra, Hexagonal wurtzite structure

I. INTRODUCTION

Aluminum-doped zinc oxide (AZO) nanostructures have garnered significant interest in recent years due to their unique combination of structural, electrical, and optical properties.

These properties make AZO nanostructures highly suitable for many applications, including transparent conductive oxides (TCOs), gas sensors, photovoltaic devices, and light-emitting diodes (LEDs) [1,2]. The co-precipitation method, a relatively simple and cost-effective synthesis technique, has been widely employed to produce AZO nanostructures with controlled morphology and doping levels, further enhancing their application potential. The structural characteristics of AZO nanostructures, such as crystal size, lattice parameters, and morphology, significantly influence their performance in various applications. Studies have shown that aluminum doping can alter ZnO's crystallinity and grain size, leading to improved mechanical stability and enhanced surface area, which are crucial for sensor applications [3,4].The co-precipitation method allows for precise control over these structural parameters, facilitating the optimization of nanostructures for specific uses. The electrical properties of AZO nanostructures, including conductivity and carrier concentration, are pivotal for their function as Transparent Conductive Oxides (TCOs) and in electronic devices [5].

Transparent Conductive Oxides (TCOs): AZO nanostructures are extensively used as TCOs in solar cells, touch screens, and flat-panel displays due to their strong electrical conductivity and optical transparency [6]. Aluminum doping introduces additional free carriers into the ZnO lattice, thereby increasing its electrical conductivity. This enhancement in electrical properties makes AZO nanostructures ideal candidates for use in thin-film transistors and other electronic components where high conductivity and transparency are required [7]. Because of their substantial absorption in the UV and great transparency in the visible spectrum, AZO nanostructures are suited for optoelectronic applications [8]. The co-precipitation synthesis allows for tuning the energy band gap of ZnO by varying the doping concentration of aluminum. This tunability is crucial for optimizing the material for specific optoelectronic devices, such as UV photodetectors and solar cells [9]. By fine-tuning these properties through controlled synthesis methods, we can develop materials tailored to specific technological needs, paving the way for advancements in electronics, optoelectronics, and sensor technology.

II. EXPERIMENTAL DETAILS

A. Synthesis Details

Al-doped Zinc Oxide nanopowders with composition $Al_xZn_{1-x}O$ (x = 0, 0.02, 0.04, 0.06, 0.08), were synthesized using the method of coprecipitation. Aluminum Nitrate Nonahydrate ($Al(NO_3)_3 . 9H_2O$) and Zinc Nitrate Hexahydrate ($Zn(NO_3)_2 . 6H_2O$) are the starting materials for this procedure. The raw materials were purchased from Sigma and were utilized straight out of the container, without any further purification. To get the precursor solution, the starting chemicals were first dissolved in 250 mL of deionized water in accordance to the stoichiometric ratio. The mixture was then stirred for six hours at a speed of about 2000 rpm using a 5 mL Remi magnetic stirrer. Then, Sodium Hydroxide (NaOH) solution was slowly added until the metal nitrate solution's pH reached 10. The pH of the solution is selected after careful examination of how pH impacts ZnO's properties. After some time of continuous stirring for 6 hours, a transparent, colorless, and uniform sol was formed. In the next step, the mixture was continuously stirred while the temperature was kept at 80° for three hours. Afterward, a centrifuge was used to repeatedly wash the precipitate to remove any last traces of nitrates from the mixture. The synthesized product was then filtered through paper Whatman filter No. 42 and heated for 12 hours at 350 °C in a muffle furnace. With the help of an agate mortar and pestle, the heat-treated powders were refined to fine powder before being submitted for various characterizations. An illustration of the nanopowder synthesis is represented in Figure 1.

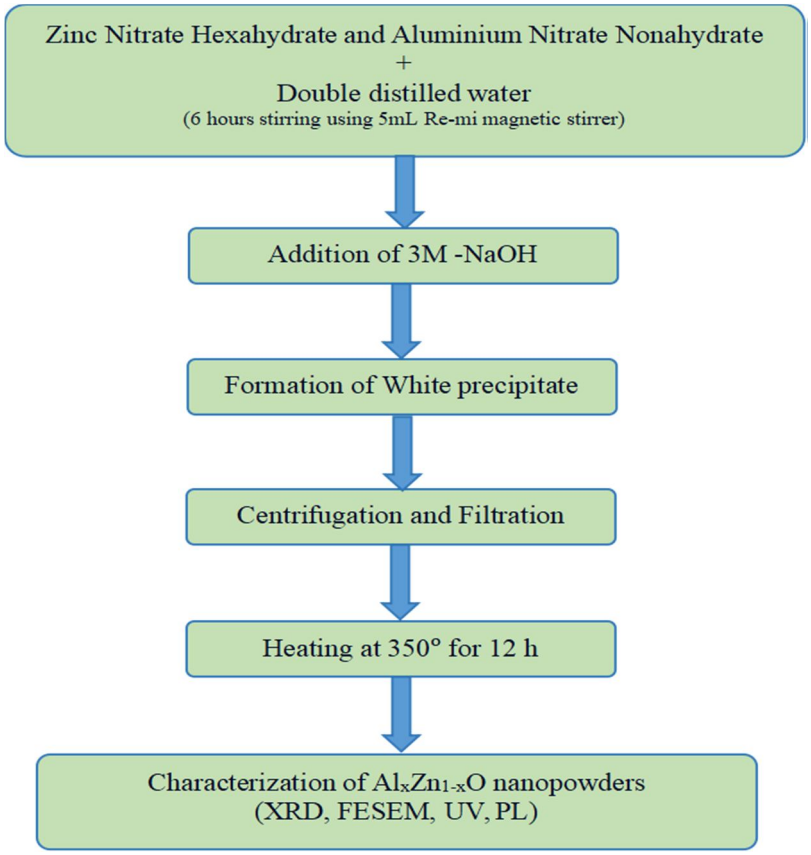

Figure 1: Synthesis of $Al_xZn_{1-x}O$ nanopowders

B. Characterization

The produced powders' optical, morphological, and structural properties were characterized using different techniques. X-ray diffraction (XRD) [Philips PAN analytical, PW1830] is employed to measure the structural information of the synthesized nanopowders. Field Emission Scanning Electron Microscopy (FESEM; Make:Carl Zeiss; Model: Neon.40) determines the powder particle size and morphology. A Shimadzu UV 1800 UV–visible spectrometer tests the optical absorption characteristics of produced powders at room temperature, with measurement range included 200–800 nm, with a resolution of 4 nm. To provide insight into several faults in the produced powders, room-temperature Photoluminescence (PL; Horibs Jobin Yvon Fluorolog-3) spectroscopy is captured at an excitation wavelength of 350 nm (Energy = 3.54eV).

III. RESULTS AND DISCUSSION

A. XRD Analysis

Figure 2 represents powder XRD patterns of the investigated samples, recorded using Cu Kα radiation within the angle range of 10-80°. The diffraction peaks are noticed around 31.99°, 34.65°, 36.47°, 47.73°, 56.79°, 63.07°, 66.55°, 68.14°, and 69.27° angles. These peaks and their corresponding planes confirm the characteristic ZnO's hexagonal wurtzite crystal structure as described in card number 36-1451 of JCPDS.

The high intense diffraction peaks in the XRD patterns confirm high crystallinity and the broadening FWHM confirms the low crystalline nature. It also observed the phase purity of the synthesized powders as there were no additional impurity-corresponding diffraction peaks. With the substitution of Al, there is a small change in the FWHM and peak position with relation to pure ZnO. The low angle shift for 2% Al substitution is higher than the others. The inconsistent peak shift with the substitution is attributed to changes in the crystallographic properties of the samples, which are caused by the significant differences in the ionic radii of Zn (0.74 Å) and Al (0.53 Å). The shift in the peak position with the dopants is discussed by several authors [10,11]. The reports conclude that the host and substituted ionic radii play a major role in shifting the position of the peak toward the left or right compared to the original one [12,13].

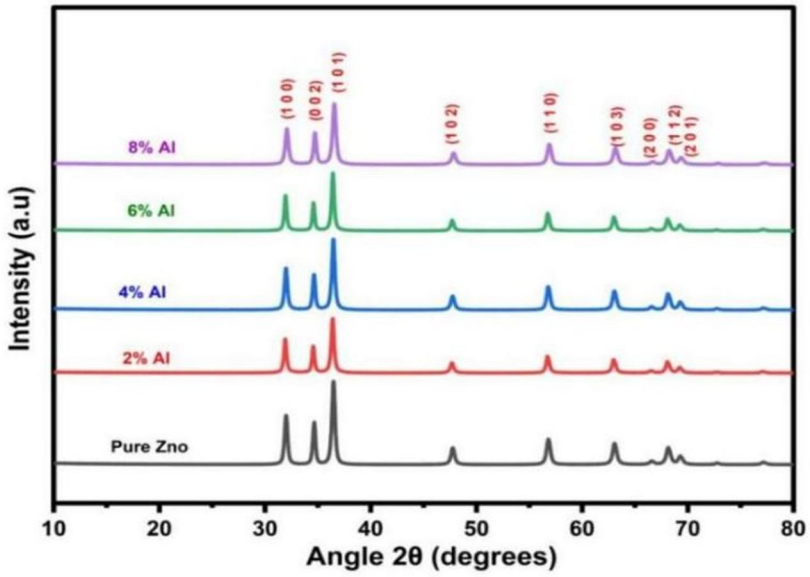

Figure 2: XRD patterns of $Al_xZn_{1-x}O$ nanopowders

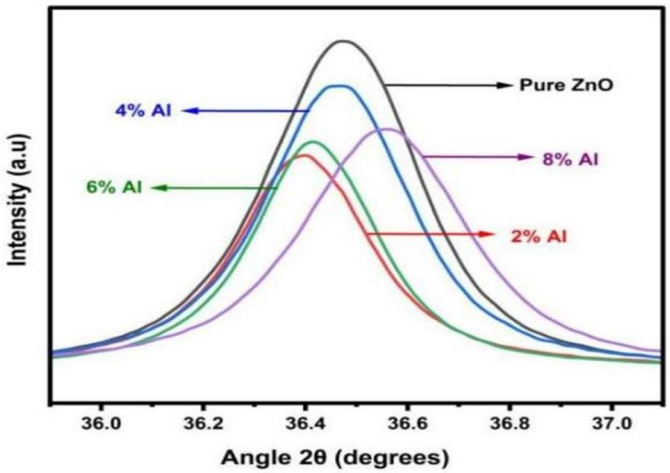

Figure 3: A shift of hexagonal (1 0 1) Bragg's peak at 2θ=35.8 °– 37.2°

Bragg's law represented as equation 1 used to calculate the structural parameters of $Al_xZn_{1-x}O$ nanopowders by using the following relations (2–3) and values are represented in Table I.

$$2d\,Sin\theta = n\lambda \text{ ---------- (1)}$$

Lattice parameters "a" and "c" were evaluated by analyzing diffraction peaks which, in turn, correspond to the (1 0 0) and (0 0 2) planes through the following relations.

$$a = \frac{\lambda}{\sqrt{3}\,Sin\theta} \text{ ---------- (2)}$$

$$c = \frac{\lambda}{Sin\theta} \text{ ---------- (3)}$$

Sample	2θ°	d-Spacing	a	c	c/a	D
Pure ZnO	36.47149	2.46159	3.22812	5.17409	1.602816	22.2435
2% Al	36.39621	2.46651	3.23565	5.18610	1.602801	22.2829
4% Al	36.46110	2.46227	3.22905	5.17645	1.603089	22.4919
6% Al	36.41780	2.46510	3.23354	5.18300	1.602891	25.5552
8% Al	36.55300	2.45629	3.21962	5.16314	1.603646	19.7473

TABLE I: LATTICE PARAMETERS OF $Al_XZn_{1-X}O$ NANOPOWDERS

The crystallite sizes (D) along with structural parameters were measured for $Al_xZn_{1-x}O$ nanopowders using the known Scherrer equation (4) and there are somewhat higher crystallite sizes observed with 2%, 4% and 6% Al substitution and on contrast, 8% Al substitution decreased the crystallite size in comparison with pure ZnO as given in Table I.

$$D = \frac{k\lambda}{\beta cos\theta} \text{ ---------- (4)}$$

B. FESEM Examination

Figure 4 presents the Field Emission Scanning Electron Microscopy (FESEM) images of $Al_xZn_{1-x}O$ powders, captured at a scale of 200 nm and a magnification of 100,000 times. The images reveal distinct morphological characteristics for $Al_xZn_{1-x}O$ nanopowders. In case of pure ZnO, the nanoparticles exhibit a well-defined hexagonal shape, indicative of their intrinsic crystal structure. However, with the incorporation of Al^{3+} ions, there is a notable transformation in the nanoparticle morphology from hexagonal to spherical shapes.

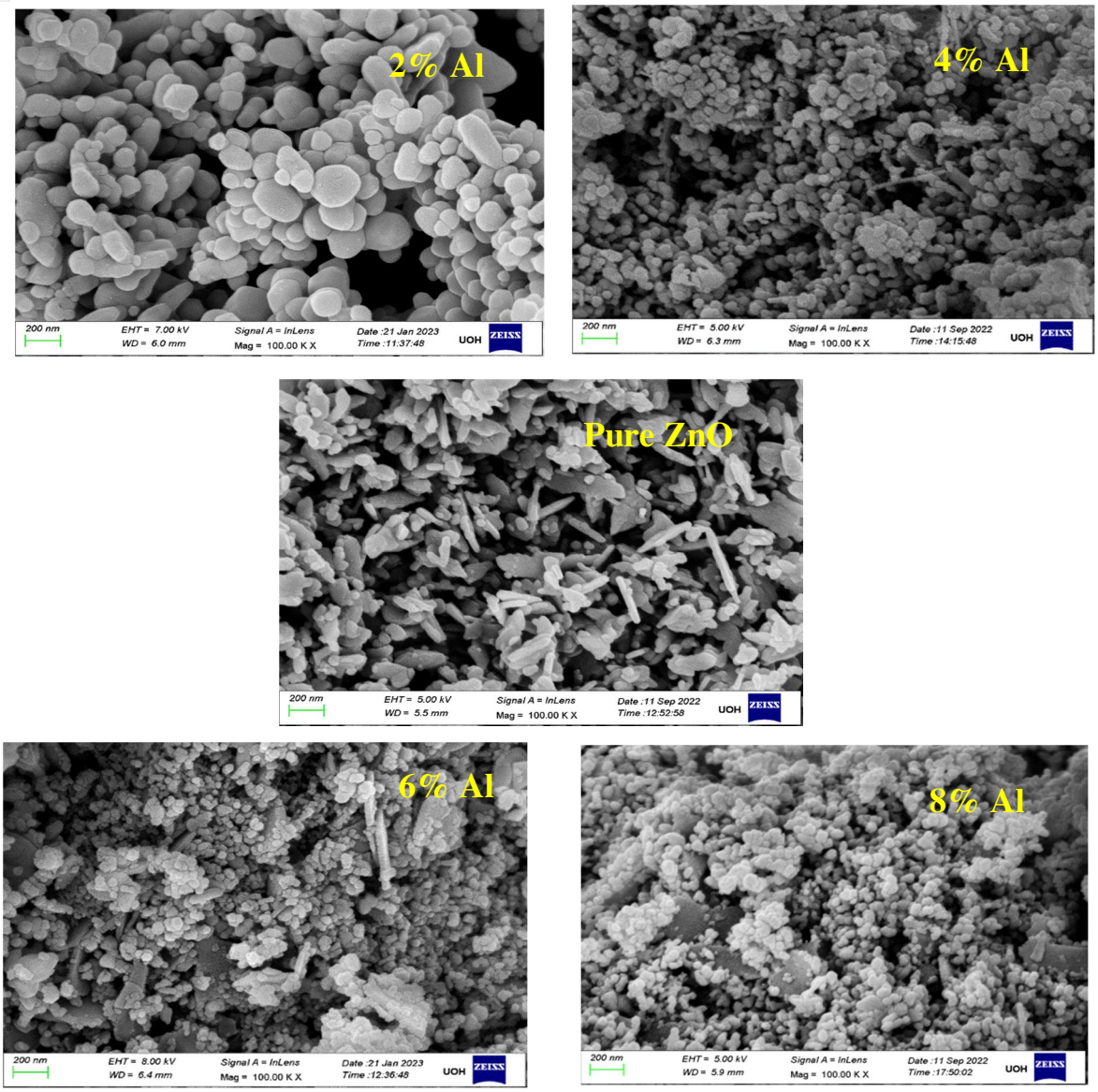

Figure 4: FESEM Images of $Al_xZn_{1-x}O$ powders at 200nm scale and 100,000x Magnification

This significant variation in surface shape indicates that the development process of ZnO nanopowders is greatly influenced by the presence of Al^{3+} ions. The introduction of Al^{3+} ions likely disrupts the regular hexagonal lattice, leading to the formation of spherical nanoparticles. Such morphological changes imply that the dopant concentration of Al^{3+} directly impacts the structural evolution of ZnO during the synthesis process [14–16] . These observations align with the research results published in the literature. Research has demonstrated that introducing different elements into ZnO may cause considerable changes to its morphological and structural characteristics, which is consistent with the findings of our FESEM investigation. The transformation from hexagonal to spherical morphology due to Al^{3+} doping aligns with the reported effects of dopants on ZnO's growth and morphology [17].

C. UV- Vis Spectroscopy Analysis

Nanopowders exhibit unique optical properties influenced by their size, shape, concentration, agglomeration state, and refractive index, particularly near the nanoparticle surface. Utilizing these properties, UV-Vis spectroscopy is a crucial method for identifying, characterizing, and studying nanomaterials [17]. The UV-Vis spectrum of $Al_xZn_{1-x}O$ nanopowders, illustrated in Figure 5, highlights distinct features, with a significant absorption band at approximately 353 nm. This absorption is attributed to the composition and structure of the nanopowders.

An excitonic absorption peak appears around 250 nm for the ZnO nanopowders, and will lie well below the band gap wavelength of 358 nm (corresponding to an energy gap of Eg = 3.46 eV). This highlights the relationship between the nanopowder's composition and its optical properties.

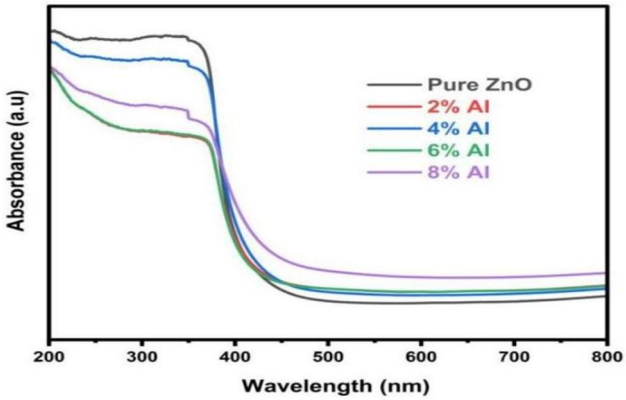

Figure 5: UV-Vis spectra of $Al_xZn_{1-x}O$ nanopowders

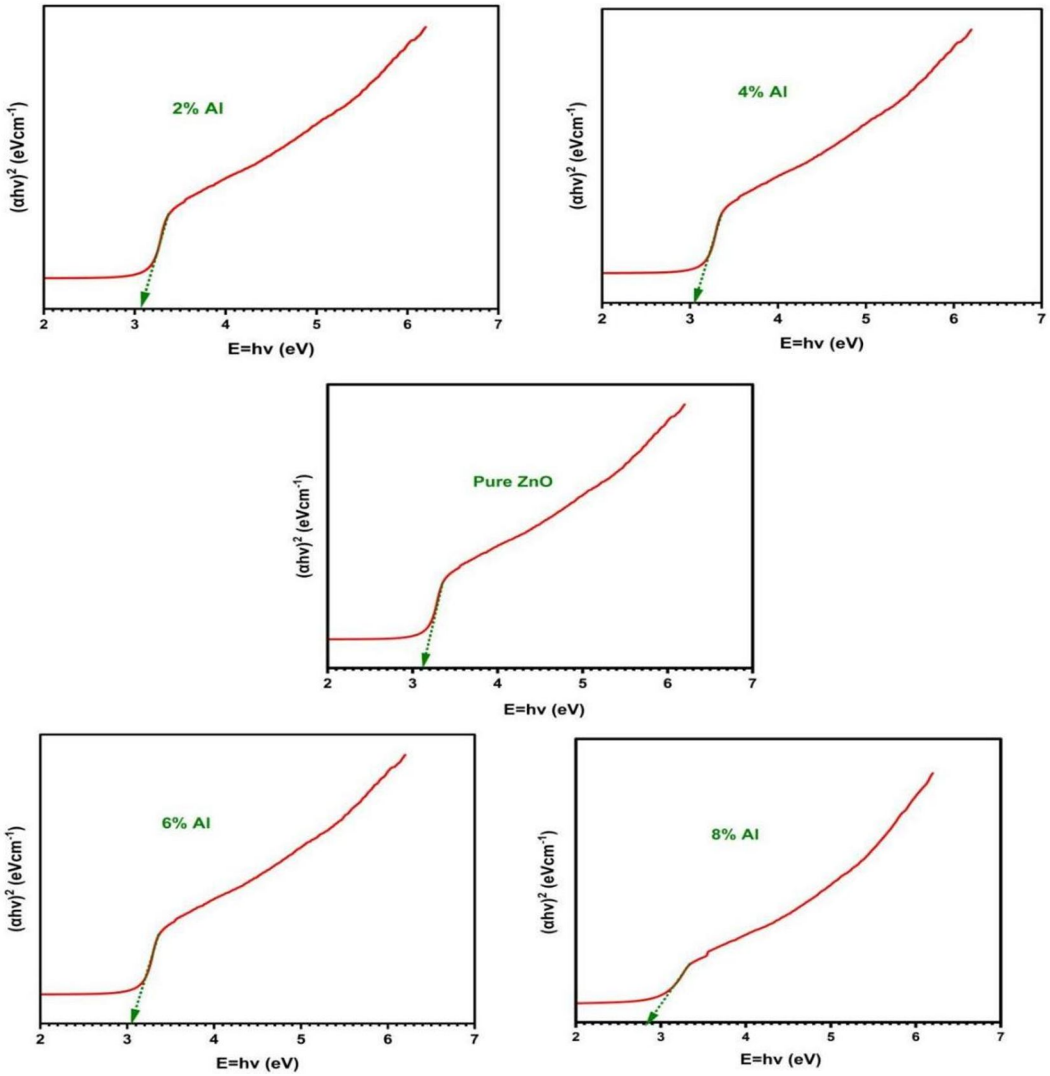

Figure 6: Tauc plot of $Al_xZn_{1-x}O$ nanopowders

Determining the energy gap (Eg) of materials is essential for understanding their electronic properties and potential applications. It is typically done using Tauc plots, which correlate the square of the absorption coefficient (αhv) with the photon energy (hv). Figure 6 illustrates the Tauc plots obtained for $Al_xZn_{1-x}O$ nanopowders. The energy gap values obtained for different compositions of $Al_xZn_{1-x}O$ nanopowders are significant indicators of their electronic structure. The energy gaps for pure ZnO, and for ZnO with 2%, 4%, 6%, and 8% Al were 3.14, 3.08, 3.04, 3.03, and 2.84 eV respectively. These values provide insights into how aluminum incorporation affects the band structure of ZnO and influences its optical properties. A notable observation in determining the energy gap is the effect of annealing on the sample. It is hypothesized that the variation in the energy gap value post-annealing is due to the enlargement of grain structures within the nanopowders. This highlights the influence of processing conditions on the material's optical properties and the importance of annealing in optimizing these properties for specific applications.

D. Photo Luminescence Spectroscopy Analysis

Photoluminescence (PL) studies are crucial for characterizing a range of material properties, such as the duration of excited states, surface contact locations, and impurity levels. PL emission provides both extrinsic and intrinsic flaws information simultaneously. Figure 7 displays the photoluminescence spectra of each sample, obtained at an excitation wavelength of 350 nm.

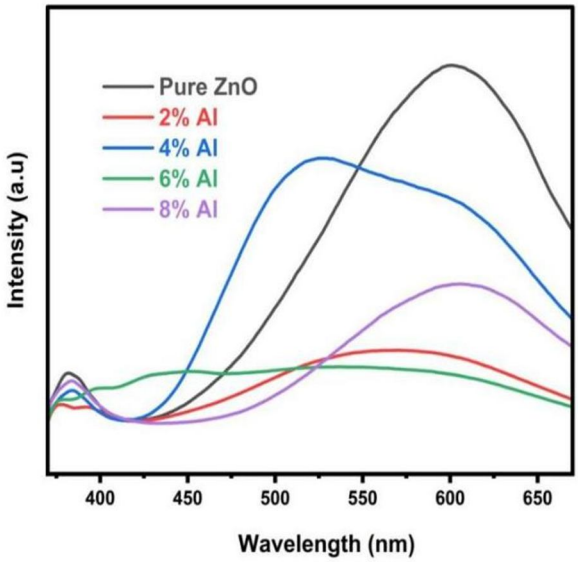

Figure 7: PL spectra of $Al_xZn_{1-x}O$ nanopowders

The PL spectra of $Al_xZn_{1-x}O$ nanopowders show two prominent PL peaks associated with the visible deep-level emission (DLE) and the UV near-band-edge (NBE) emission. The UV NBE emission, indicative of near-band gap excitonic emission or band-to-band transition, results from the recombination of free excitons. This emission is attributed to the inter-band radiative recombination between holes in the valence band and photogenerated electrons in the conduction band. The UV emission peak for the 2% Al and 6% Al nanopowders shows a slight blue shift, as shown in Figure 7. This shift is attributable to an increase in nonradiative recombination. Conversely, Figure 7 shows a minor red shift in the UV NBE emission peak location for 4% and 8% Al nanopowders. Fonoberov and Balandin proposed two theories to explain the redshift of UV NBE emission in ZnO nanoparticles: excitons associated with an ionized impurity at the nanoparticle surface or excitons trapped within the nanoparticle. The red shift in our samples is attributed to the size effect on the energy level of trapped excitons, as the average size of nanopowders increased with annealing temperature. Inherent defects such as oxygen vacancies (VO), singly negatively charged Zn vacancies (VZn), interstitial zinc (Zni), and zinc vacancies (VZn) are associated with the DLE. The second emission might result from the radiative recombination of a photogenerated hole with an electron filling an oxygen vacancy. According to earlier publications, the results in Table I are supported by the suggestion that the lattice parameters of the ZnO system are increased by the presence of both Zi and Oi sites by Al doping. The PL spectra, however, suggest that as the lattice parameters increase, the involvement of the Oi sites becomes more apparent. Overall, the considerable point-defect development in ZnO nanopowders may be designed via Al doping.

IV. CONCLUSION

In conclusion, the study demonstrates that Al-doped ZnO nanopowders exhibit several enhanced parameters when compared to undoped ZnO. Notably, the crystallite size of the nanopowders decreases as the doping percentage of Al increases, reaching an optimal reduction at 8% Al doping. The analysis of structural and lattice parameters reveals significant impacts on various material properties, suggesting that Al doping effectively modifies the crystal structure of ZnO. Furthermore, the phase purity of the samples was confirmed, with no detectable impurities present in the compound. An important finding is that the increase in Al doping percentage correlates with a decrease in the energy gap of ZnO, which may have implications for its electronic and optical applications. The photoluminescence (PL) spectrum analysis indicates that ZnO nanoparticles exhibit a strong ultraviolet (UV) emission peak associated with near-band-edge emission, alongside a broad visible emission attributed to deep-level defects. This behavior underscores the potential of Al-doped ZnO in optoelectronic devices, where controlled doping can tailor the material's electronic and optical properties for specific applications. Overall, the results highlight the beneficial effects of Al doping on ZnO nanoparticles, paving the way for further exploration in various technological applications.

V. ACKNOWLEDGEMENT

Sowmya Kanakamedala would like to thank K.V.N. Sunitha, Principal, and Anitha HoD, BS&H, and BVRIT, Hyderabad, for their constant support in carrying out this work.

REFERENCES

[1] Mohite RM, Kothawale RR. Al-doped zinc oxide nanostructures as transparent conductive window layer for photovoltaic applications. vol. 54. 2015.
[2] M YD, Dhote DS. A Review On Applications Of Zinc Oxide Nanostructures. vol. 2. 2015.
[3] Raha S, Ahmaruzzaman Md. ZnO nanostructured materials and their potential applications: progress, challenges and perspectives. Nanoscale Adv 2022;4:1868–925. https://doi.org/10.1039/D1NA00880C.
[4] Aydın H, Yakuphanoglu F, Aydın C. Al-doped ZnO as a multifunctional nanomaterial: Structural, morphological, optical and low-temperature gas sensing properties. J Alloys Compd 2019;773:802–11. https://doi.org/10.1016/j.jallcom.2018.09.327.
[5] Zhang W, Gan J, Li L, Hu Z, Shi L, Xu N, et al. Tailoring of optical and electrical properties of transparent and conductive Al-doped ZnO films by adjustment of Al concentration. Mater Sci Semicond Process 2018;74:147–53. https://doi.org/10.1016/j.mssp.2017.10.028
[6] Lewis BG, Paine DC. Applications and Processing of Transparent Conducting Oxides. MRS Bull 2000;25:22–7. https://doi.org/10.1557/mrs2000.147.
[7] Amri A, Arab L, Meftah A, Latif A. Effect of aluminum doping on the structural, optical and electrical properties of ZnO thin films processed under thermal shock conditions. Results in Optics 2023;11:100426. https://doi.org/10.1016/j.rio.2023.100426.
[8] Khan MdI, Neha TR, Billah MdM. UV-irradiated sol-gel spin coated AZO thin films: enhanced optoelectronic properties. Heliyon 2022;8:e08743. https://doi.org/10.1016/j.heliyon.2022.e08743.
[9] Kaur M, Kaur P, Kaur G, Dev K, Negi P, Sharma R. Structural, morphological and optical properties of Eu-N co-doped zinc oxide nanoparticles synthesized using co-precipitation technique. Vacuum 2018;155:689–95. https://doi.org/10.1016/j.vacuum.2018.06.046.
[10] Rajesh Kumar B, Hymavathi B. X-ray peak profile analysis of solid-state sintered alumina doped zinc oxide ceramics by Williamson–Hall and size-strain plot methods. Journal of Asian Ceramic Societies 2017;5:94–103. https://doi.org/10.1016/j.jascer.2017.02.001
[11] Farha AH, Al Naim AF, Mazher J, Nasr O, Alouane MHH. Structural and Optical Characteristics of Highly UV-Blue Luminescent ZnNiO Nanoparticles Prepared by Sol–Gel Method. Materials 2020;13:879. https://doi.org/10.3390/ma13040879.
[12] Sowmya K, Aparna Y, Prakash AC, Ramesh T. Impact of pH on structural, morphological, optical, and magnetic properties of zinc oxide nanopowders synthesized by co-precipitation method. Journal of Materials Science: Materials in Electronics 2024;35:972. https://doi.org/10.1007/s10854-024-12548-x.
[13] Sowmya K, Aparna Y, Chendra Prakash A, Thotakura R, Bhaskar A. Influence of Metal (Al, Mg, Sm, and Cu) Dopants on Structural, Optical, Magnetic, and Antimicrobial Properties of ZnO Nanopowders Synthesized by Coprecipitation Method. Physica Status Solidi (a) 2024;221. https://doi.org/10.1002/pssa.202300628.
[14] Alexieva G, Lovchinov K, Petrov M, Gergova R, Tyutyundzhiev N. Influence of Al Doping on the Morphological, Structural and Gas Sensing Properties of Electrochemically Deposited ZnO Films on Quartz Resonators. Coatings 2022;12:81. https://doi.org/10.3390/coatings12010081.
[15] Chen JT, Wang J, Zhuo RF, Yan D, Feng JJ, Zhang F, et al. The effect of Al doping on the morphology and optical property of ZnO nanostructures prepared by hydrothermal process. Appl Surf Sci 2009;255:3959–64. https://doi.org/10.1016/j.apsusc.2008.10.086.
[16] Sridhar A, Sakthivel P, Saravanakumar K, Sankaranarayanan RK. Dual doping effect of Ag+ & Al3+ on the structural, optical, photocatalytic properties of ZnO nanoparticles. Applied Surface Science Advances 2023;13:100382. https://doi.org/10.1016/j.apsadv.2023.100382.
[17] Akdağ A, Budak HF, Yılmaz M, Efe A, Büyükaydın M, Can M, et al. Structural and Morphological Properties of Al doped ZnO Nanoparticles. J Phys Conf Ser 2016;707:012020. https://doi.org/10.1088/1742-6596/707/1/012020.

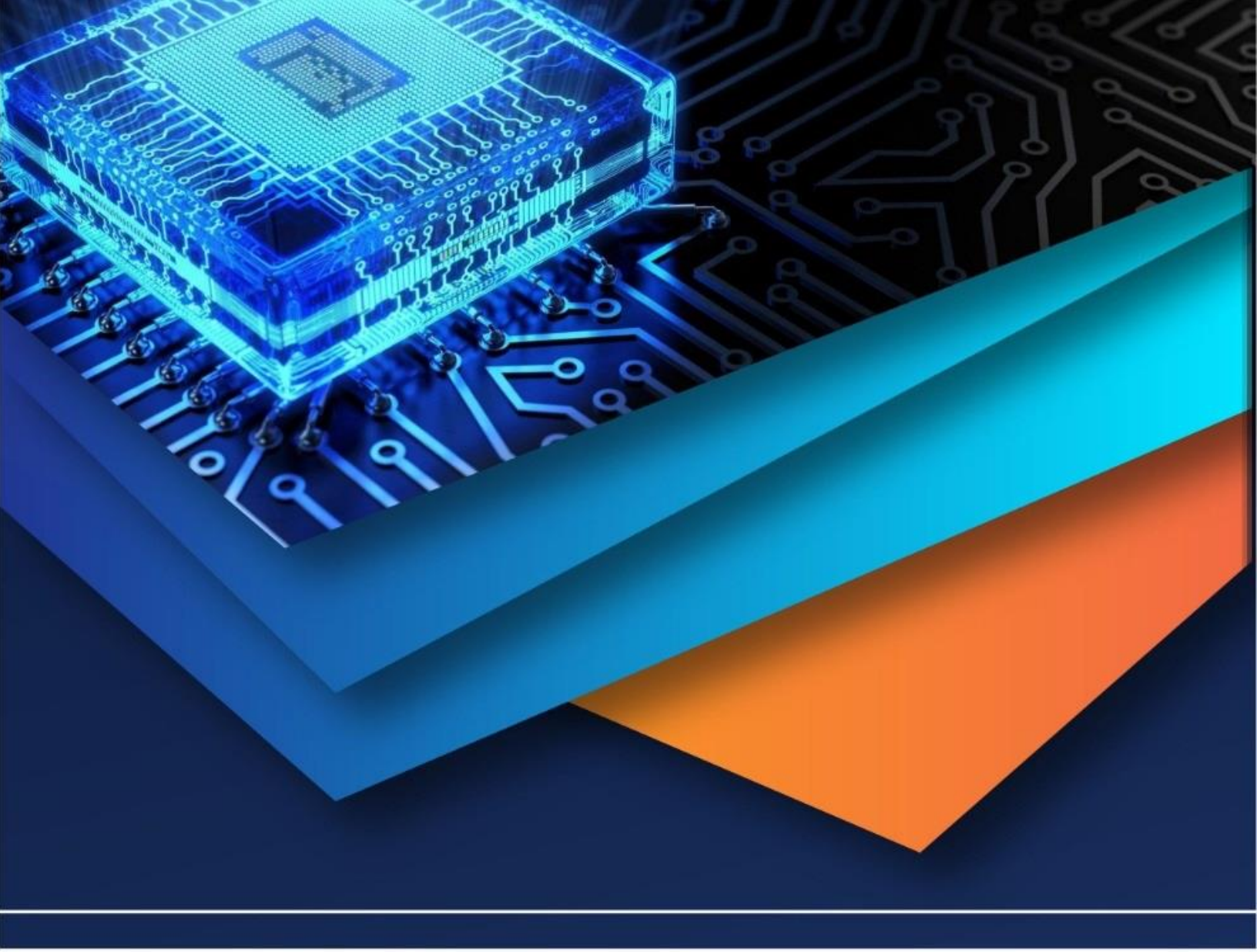

10.22214/IJRASET

45.98

IMPACT FACTOR: 7.129

IMPACT FACTOR: 7.429

INTERNATIONAL JOURNAL FOR RESEARCH

IN APPLIED SCIENCE & ENGINEERING TECHNOLOGY